Supplementary Information for

Molecular Imaging of Chemokine-Like Receptor 1 (CMKLR1) in Experimental Acute Lung Injury

Philip Z. Mannes, Clayton E. Barnes, Jana Biermann, Joseph D. Latoche, Kathryn E. Day, Qin Zhu, Mohammadreza Tabary, Zeyu Xiong, Jessie R. Nedrow, Benjamin Izar, Carolyn J. Anderson, Flordeliza S. Villanueva, Janet S. Lee, Sina Tavakoli*

*Corresponding author. Email: sit23@pitt.edu

This PDF file includes:

Supplementary Methods

Figs. S1 to S13

Tables S1 to S7

Materials and Methods

Chemicals and reagents

The major chemicals and reagents (Table S1), plasmids (Table S2), HPLC methods (Table S3), flow cytometry reagents (Table S4), histology antibodies (Table S5), Taqman primers (Table S6), and details of publicly available single-cell RNA sequencing datasets (Table S7) are listed in the Supplementary Information.

Tracer synthesis and characterization

NODAGA-CG34, $Chem_{145-157}$ and 6CF-$Chem_{145-157}$ were synthesized by the University of Pittsburgh Peptide and Peptoid Synthesis Core Facility. NODAGA-CG34 (NODAGA-Ahx-Y-Cha-Hyp-G-Cit-F-a-Tic-S-COOH) synthesis was performed on a Liberty CEM microwave synthesizer using fluorenylmethyloxycarbonyl (Fmoc) chemistry at a 0.1 mmol scale. Stepwise addition of each Fmoc-protected amino acid to p-alkoxybenzyl alcohol (Wang) resin was accomplished using ethyl-(2Z)-2-cyano-2-hydroxyiminoacetate/N,N-Diisopropylcarbodiimide (Oxyma/DIC) activation chemistry. Upon completion of peptide chain assembly, the N-terminal amino group of the peptide resin was manually coupled with 6-(Fmoc-amino)hexanoic acid (Fmoc-6-Ahx-OH) using N,N-diisopropylethylamine/N,N,N′,N′-tetramethyl-O-(benzotriazol-1-yl)uronium tetrafluoroborate/1-hydroxybenzotriazole (DIPEA/TBTU/HOBt) for 2 hours at room temperature. Manual deprotection of the final Fmoc group using 20% piperidine was followed by on-resin attachment of NODAGA-NHS (5 eq.) in DIPEA / N,N-dimethylformamide (DMF) for 2 hours at room temperature. Cleavage of NODAGA-CG34 from the Wang resin was performed using trifluoroacetic acid (TFA): triisopropylsilane:H_2O (TFA:TIPS:H_2O) (90:25:25) for 2 hours at room temperature followed by precipitation in diethyl Ether (Et_2O). The resulting crude peptide was purified by preparative C-18 RP-HPLC on a Waters Delta Prep 4000 chromatography system and standard acetonitrile (ACN) / 0.1%TFA gradient conditions. Analytical C-18 RP-HPLC characterization on a Waters Alliance chromatography system followed by high resolution mass spectrometry (HRMS) using a Thermo Scientific Q-Exactive Oribtrap (Mass Spectrometry Lab, University of Pittsburgh) confirmed the expected purity (>95%) and mass of the final product (FTMS -p ESI, Expected $C_{77}H_{108}O_{22}N_{15}$ = 1594.77879, found 1594.78165), respectively. The characterization for NODAGA-CG34 (NODAGA-Ahx-Y-Cha-Hyp-G-Cit-F-a-Tic-S-COOH) is shown in Fig. S1 and Fig. S2. Two additional peptides, $Chem_{145-157}$ (P-H-S-F-Y-F-P-G-Q-F-A-F-S-COOH) and 6CF-$Chem_{145-157}$ (6-carboxyfluorescein-P-H-S-F-Y-F-P-G-Q-F-A-F-S-COOH) were also synthesized using related solid phase peptide chemistry and were similarly characterized using HPLC and mass spectrometry.

Cell culture

HeLa cells were grown in complete growth media formulated as Dulbecco's Modified

Eagle Medium (DMEM) supplemented with 10% fetal bovine serum (FBS) and 1% penicillin/streptomycin. Resident peritoneal cells were harvested from C57BL/6J mice, as previously described, via peritoneal lavage with PBS (1).

Transient transfection

HeLa cells at 70-90% confluency were transiently transfected with mouse CMKLR1 and/or $G_{\alpha 15}$ cDNA plasmids using Lipofectamine 3000 according to manufacturer's instructions. Co-transfections of mouse CMKLR1 and $G_{\alpha 15}$ were conducted at a ratio of 4:1. On day one post-transfection, cells were seeded on poly-D-lysine coated black or clear 96-well plate for calcium mobilization or radioligand bind assays, respectively, at a density of ~40,000 cells/well. The transfected cells were grown in complete growth media until use in a calcium flux or radioligand binding assay on day two post-transfection.

Calcium mobilization assay

The calcium flux assay was performed according to the manufacturer's instructions with minor modifications. HeLa cells transiently transfected with mouse CMKLR1 and/or $G_{\alpha 15}$ were washed with assay buffer (HBSS with Ca^{+2} and Mg^{+2}, supplemented with 20 mM HEPES and 2 mM probenecid), and loaded with Fluo-4 AM dye dissolved in loading buffer (assay buffer supplemented with 2.5 µM Fluo-4 and 0.2% Pluronic F-127) for 30 minutes at 37 °C in the dark. Then, cells were washed twice and incubated with assay buffer. A baseline fluorescence measurement was recorded by a Synergy H4 Hybrid Multi-Mode Microplate Reader (Biotek) using the following parameters for 4 minutes: excitation: 490 nm, emission: 515 nm, bandwidths: 9 nm, and frequency: 10 seconds. Subsequently, cells were stimulated with different concentrations of either NODAGA-CG34 or $Chem_{145-157}$, and kinetic fluorescent measurements were performed every 10 seconds for 4 minutes. The maximum response values (F) were normalized to baseline values (F_0) for each well with the following equation: response = F/F_0. Dose-response curves were generated using GraphPad Prism 9 Software.

Radiolabeling

NODAGA-CG34 in radiolabeling buffer (0.5 M NaOAc buffer pH = 6.9 and 0.8 mM gentisic acid dissolved in water) and [^{64}Cu]$CuCl_2$ in 0.1 M HCl (37 MBq per 1.0 nmol of NODAGA-CG34) were added to a low protein retention Eppendorf tube. The pH was checked to ensure pH ~6.5 – 7.0, and then the radiolabeling reaction was allowed to proceed at 40 °C for 30 minutes. The radiochemical purity of [^{64}Cu]NODAGA-CG34 was determined by radio-HPLC to confirm a minimum purity of >95% prior to use in all *in vitro* and *in vivo* experiments. Relevant radio-HPLC methods are described in Table S3.

Radioligand binding assay

HeLa cells transiently transfected with mouse CMKLR1 were washed with a binding buffer (50 mM HEPES, 1.0 mM $CaCl_2$, 5.0 mM $MgCl_2$, 0.5% BSA, pH: 7.5). Cells were then incubated at room temperature in the binding buffer with [^{64}Cu]NODAGA-CG34 (0 to 1,000 nM) in the absence or presence of 2.5 µM $Chem_{145-157}$ to measure total and non-specific binding, respectively. After 1 hour, cells were washed twice with ice-cold binding buffer and lysed with 0.2 M NaOH / 1% SDS. The radioactivity of cell lysates was quantified in a γ-counter (Wizard2, PerkinElmer). The total, non-specific, and specific saturation binding curves were generated (2) using GraphPad Prism 9 Software.

Mouse model of experimental lung injury

Animal experiments were performed on C57BL/6J mice under a protocol approved by the institutional animal care and use committee. Adult 9- to 12-week-old C57BL/6J mice (Jackson Laboratory, strain # 000664) were used throughout the study. Mice were administered intratracheally with 2.5 µg/g LPS from *Escherichia coli* O111:B4 in 60 µl of phosphate-buffered saline (PBS) to induce lung injury (3). Control mice were intratracheally injected with 60 µl of PBS. In experiments involving anti-inflammatory treatment, mice receiving dexamethasone were given two doses of 10 mg/kg (in 500 µL in PBS) via intraperitoneal injections at 1 and 24 hours following LPS instillation, whereas control mice were treated with intraperitoneal PBS (500 µL) injections. Mice were euthanized two days after the induction of lung injury. Studies were performed in accordance with a protocol approved by the University of Pittsburgh Institutional Animal Care and Use Committee.

Measurement of octanol/water partition coefficient (logD)

Approximately 1.48 MBq of [^{64}Cu]NODAGA-CG34 (in 5 µL) was added to a 1 mL mixture of 1-octanol (500 µL) and PBS (500 µL). The mixture was vigorously vortexed for one minute and then centrifuged at 1,000 rpm for 5 minutes. The sample was then placed at room temperature for 30 minutes to allow the phases to completely separate. An equal aliquot (25-50 µL) was carefully removed from each the organic and aqueous layers and counted with a γ-counter (Wizard^2, PerkinElmer). The octanol/water partition coefficient (logD) was calculated as: log([^{64}Cu]NODAGA-$CG34_{Octanol}$ / [^{64}Cu]NODAGA-$CG34_{PBS}$).

Plasma stability assay

Plasma stability assay was performed according to previous reports (4) with minor modifications. [^{64}Cu]NODAGA-CG34 (~22 – 26 MBq in 70 µL of radiolabeling buffer) was added to 700 µL of C57BL/6 mouse plasma (Innovative Research). The mixture was incubated at 37 °C. At specific time points, an aliquot of ~60 µL (0, 2, and 4 hours) or 100

µL (19 hours) was removed, diluted with acetonitrile (> 1:1 plasma/radiotracer: acetonitrile), and centrifuged at 14,000 g for 5 minutes. Supernatant was carefully removed and diluted up to 200 µL with water and analyzed by radio-HPLC using the method described above.

Plasma protein binding assay

Plasma protein binding assay was performed per previous reports (5) with minor modifications. [^{64}Cu]NODAGA-CG34 (1.0 µL undiluted from radiolabeling stock, ~0.185 MBq) was added to 50 µL of mouse plasma. The mixture was briefly vortexed and incubated at 37 °C. At 15 or 90 minutes after incubation, 25 µL of the plasma/radioligand mixture was carefully added to the resin of a prepared (protocol from manufacturer) G50 Microspin column. The samples were centrifuged at 2,000 *g* for 2 minutes. The radioactivity in both the eluent and remaining on the column were counted with a γ-counter (Wizard2, PerkinElmer). Plasma protein binding was calculated as follows: [^{64}Cu]NODAGA-CG34$_{eluent}$ / ([^{64}Cu]NODAGA-CG34$_{eluent}$ + [^{64}Cu]NODAGA-CG34$_{column}$).

Radiolysis stability measurement

Undiluted samples of [^{64}Cu]NODAGA-CG34 in radiolabeling buffer (~ 37 MBq/0.100 mL of initial activity) were left overnight at room temperature. The following morning, an aliquot of [^{64}Cu]NODAGA-CG34 (~ 1.1 – 1.9 MBq) was analyzed by radio-HPLC to evaluate radiolysis.

PET/CT and quantification of [^{64}Cu]NODAGA-CG34 uptake

Mice treated with intratracheal instillation of LPS or PBS and untreated control mice were injected intravenously with [^{64}Cu]NODAGA-CG34 (6.41±0.05 MBq). Tracer specificity was addressed by co-injection of [^{64}Cu]NODAGA-CG34 and 100-fold molar excess of non-radiolabeled NODAGA-CG34. Static PET (~10-min) and CT (180 projections, 140-msec exposure, 180° rotation, 80-kVp, 500-µA, field-of-view: 78.5 x 100-mm) were performed, according to our previous experiments (3) (Inveon, Siemens), 90 minutes after [^{64}Cu]NODAGA-CG34 injection.

Regions of interest were drawn over the left and right lungs, and the uptake in the left and right lungs of [^{64}Cu]NODAGA-CG34 was averaged and quantified as the mean and maximal standardized uptake value (SUV_{mean} and SUV_{max}) (IRW software). Biodistribution was performed by γ-counting (Wizard2, PerkinElmer) of harvested organs. Data are reported as percentage of injected dose per gram tissue (%ID/g) after decay correction. Multiplanar reformats of PET/CT images were performed (Vivoquant software) to reconstruct planes matching the autoradiography and histology images.

[^{64}Cu]NODAGA-CG34 autoradiography of lungs

Immediately following PET/CT imaging, mice were euthanized, and the lungs were inflated with 1 mL of warmed (37 °C) optimal cutting temperature compound (OCT). Then, the lungs were placed in a block of OCT, quickly frozen, and placed at -20 °C. The following morning cryosections were cut (10 µm) and exposed to high-resolution phosphor screens (GE, BAS-IP SR2025 Super Resolution) overnight at 4 °C. Phosphor screens were scanned at 100-µm resolution using a Sapphire Biomolecular Imager.

Gene expression assays

Following PET/CT, the lungs of mice were harvested and stored for >10 half-lives at -20 °C to allow the [^{64}Cu]NODAGA-CG34 to fully decay. Then, RNA from the right lung was extracted using Trizol and converted into cDNA using reverse transcriptase according to the manufacturers' instructions. Gene expression was quantified according to standard methods (3). Quantitative real-time polymerase chain reaction (qPCR) was performed using TaqMan primers and a QuantStudio 3 system (Applied Biosystems). All transcript levels were normalized to the expression level of 18S ribosomal RNA (*Rn18s*).

Binding/uptake of 6CF-Chem$_{145\text{-}157}$ by peritoneal macrophages

Peritoneal cells were incubated in indicator-free RPMI in the presence of 6CF-Chem$_{145\text{-}157}$ (0 – 500 nM) with or without co-incubation with unlabeled Chem$_{145\text{-}157}$ (2.5 µM). Uptake of 6CF-Chem$_{145\text{-}157}$ was allowed to proceed at 37 °C for 1 hour, vortexing samples every ~15 minutes. After a single wash with PBS, flow cytometry was performed using a BD FACSCalibur (BD Biosciences) and analyzed by FlowJo software version 10.7.2 (BD Biosciences). The total, non-specific, and specific saturation binding curves were generated using GraphPad Prism 9 Software.

Competitive binding assay of 6CF-Chem$_{145\text{-}157}$ and NODAGA-CG34 in peritoneal macrophages

Peritoneal cells were incubated in indicator-free RPMI in the presence of 6CF-Chem$_{145\text{-}157}$ (100 nM) with increasing concentrations of NODAGA-CG34 ($1x10^{-10}$ M to $1x10^{-5}$ M). The competitive binding of NODAGA-CG34 and 6CF-Chem$_{145\text{-}157}$ was allowed to proceed at 37 °C for 1 hour, vortexing samples every ~15 minutes. After a single wash with PBS, flow cytometry was performed using a BD FACSCalibur (BD Biosciences) and analyzed by FlowJo software version 10.7.2 (BD Biosciences). The competitive binding curves were generated using GraphPad Prism 9 Software.

Flow cytometry for peritoneal macrophages

Peritoneal cells were incubated in indicator-free RPMI in the absence or presence of 6CF-$Chem_{145-157}$ (100 nM) with or without co-incubation with $Chem_{145-157}$ (10 µM). Uptake of 6CF-$Chem_{145-157}$ was allowed to proceed at 37 °C for 1 hour, vortexing samples every ~15 minutes. After washing with PBS, blocking was performed by 1% BSA in PBS and Fc block (2.0 µL per sample). Subsequently, a mixture of antibodies (0.5 µL per antibody per sample) was added for 0.5 hour at 4 °C. Finally, cells were washed and fixed with 4% formalin for 0.5 hour at room temperature. Flow cytometry was performed the following day using a LSR II Flow Cytometry (BD Biosciences) and analyzed by FlowJo software version 10.7.2 (BD Biosciences).

Flow cytometric immunophenotyping of murine lungs

Mice treated with intratracheal instillation of LPS or PBS and untreated control mice were euthanized and the pulmonary circulation was perfused with PBS via a right ventricular puncture. Both lungs were then minced with scissors and diluted with 5 mL of ice-cold dissociation buffer (50 mL RPMI, 1 mL FBS, and 100 µg DNase). The lungs were mechanically dissociated using a gentleMACS Dissociator (Miltenyi) using the cycle m_lung 1.02 (1X), followed by m_lung 02.01 (2X). The resulting cell suspensions were filtered using 70-µm cell strainers and red blood cells (RBC) were lysed. After counting the cells, Precision Count Beads (50 µL) were added to each sample. The cells were then divided between tubes and incubated in indicator-free RPMI in the absence or presence of 6CF-$Chem_{145-157}$ (100 nM) with or without co-incubation with $Chem_{145-157}$ (10 µM). Uptake of 6CF-$Chem_{145-157}$ was allowed to proceed at 37 °C for 1 hour, vortexing samples every ~15 minutes. After washing with PBS, cells were blocked using 1% BSA in PBS and treated first with Fc block (2.0 µL per sample), followed by a mixture of antibodies (0.5 µL per antibody per sample) and DAPI (5.0 µL 1 µg/mL per sample) for 0.5 hour at 4 °C. Finally, cells were washed and fixed with 4% formalin for 0.5 hour at room temperature. Flow cytometry was performed the following day using a LSR II Flow Cytometry (BD Biosciences) and analyzed using FlowJo software version 10.7.2 (BD Biosciences). The recovery of dendritic cells (both $CD11b^+$ and $CD11b^-$ subtypes) was low following mechanical dissociation, and they were therefore omitted from the subsequent analysis.

Lung immunostaining

Mice treated with LPS or PBS were sacrificed and the pulmonary circulation was perfused with 5 mL of PBS. Then, the lungs were inflated by intratracheal instillation of 1 mL OCT and quickly frozen. Cryosections were cut (10 µm) and fixed with cold methanol-acetone (1:1). Primary antibodies (1:200 dilution) were applied and incubated at 4 °C overnight. After washing with PBS, fluorescently conjugated secondary antibodies (1:200 dilution) were added and incubated at 4 °C for 2 hours. Slides were mounted with ProLong Gold Antifade Mountant with DAPI and photographed with an Axio Vert microscope (Zeiss).

Single-nuclei RNA sequencing (snRNA-seq) of COVID-19 and control lungs

A secondary analysis of a previously published snRNA-seq dataset from the autopsied lungs of nineteen patients with lethal COVID-19 and lung tissue (biopsy or lung resection) from seven pre-pandemic control patients without COVID-19 was performed to determine the expression of *CMKLR1* among different cell types in the lungs. The RNA sequencing data are available in the Gene Expression Omnibus (GEO) database under accession number GSE171524. Data collection and analysis were conducted as previously reported (6). Major cell populations were identified using UMAP analysis, as described in the original paper (6). The abundance and expression level of *CMKLR1* among different cell subsets were determined and compared between COVID-19 patients and controls.

Differential gene expression was performed using the Seurat (v4.1.0) (7) function 'FindAllMarkers' to identify markers in *CMKLR1*-positive and *CMKLR1*-negative cell populations. MAST algorithm was used to identify differentially expressed genes between the two groups, which were averaged across *CMKLR1*-positive and *CMKLR1*-negative cell populations for heat map representation with maximum and minimum display values clipped at 0.75 and -0.75, respectively.

Analysis of publicly available single-cell RNA sequencing (scRNA-seq) datasets for COVID-19 and cystic fibrosis

A secondary analysis of separate independently published scRNA-seq datasets (Gene Expression Omnibus accession numbers GSE145926, GSE193782, and GSE201333, or European Genome-Phenome Archive accession number EGAS00001004481) was preformed using the UCSC Cell Browser software (available at: https://cells.ucsc.edu/) (8-12). In brief, major cell populations from bronchoalveolar lavage, nasopharyngeal, airway samples, or non-airway derived tissues were identified using UMAP analysis, and the *CMKLR1* expression and abundance were compared between healthy controls, patients with COVID-19 or cystic fibrosis, or patients with other diseases.

Statistical analysis

Statistical analysis was performed using Prism 9 (GraphPad). Data are presented as mean ± SEM. A student's *t*-test was performed to compare the means values between two groups. One-way analysis of variance, followed by Fisher's Exact post hoc test, was used to compare mean values in > 2 groups. Pearson's test was used to determine the correlations between continuous variables. For snRNA-seq data, the percentage of cells positive for *CMKLR1* and the average *CMKLR1* expression in different cell subsets were compared between COVID-19 and control groups using Fisher's Exact and Wilcoxon rank-sum tests, respectively. Statistical significance was considered as $P < 0.05$.

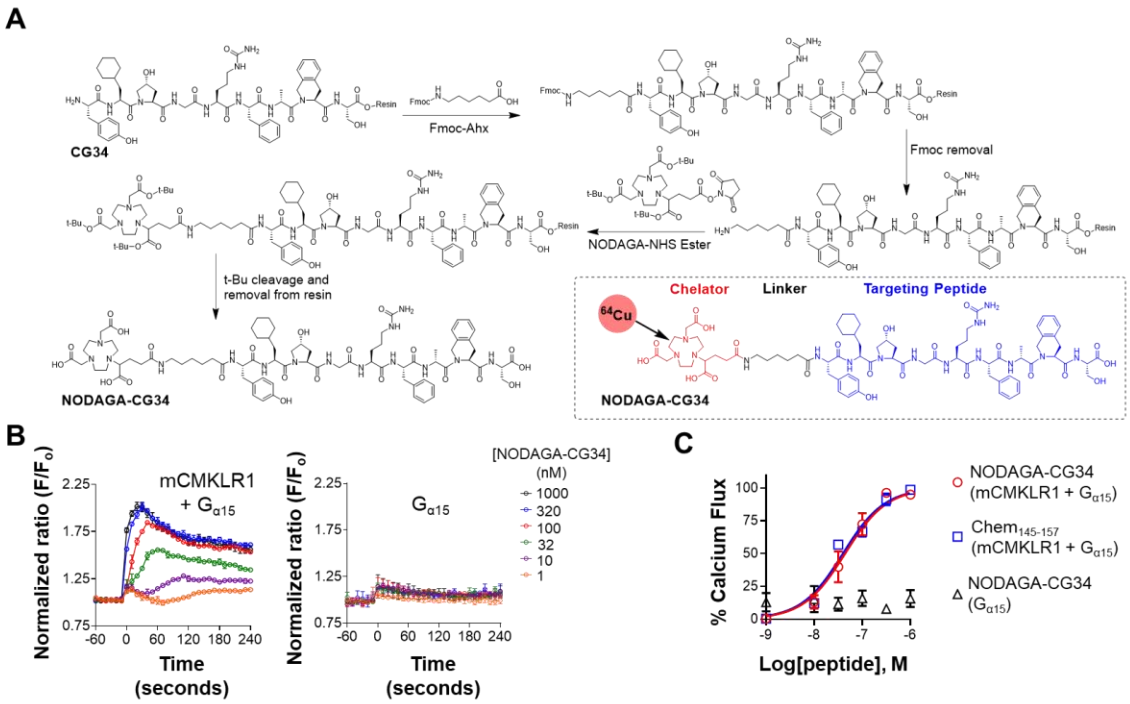

Fig S1. Synthesis and potency of NODAGA-CG34. (**A**) Synthetic overview of NODAGA-CG34 which is composed of three moieties: CMKLR1-targeting peptide (CG34), 6-aminohexanoic acid (Ahx) linker, and chelator (NODAGA). (**B**) Representative examples of Ca^{+2} mobilization assay elicited by different concentrations of NODAGA-CG34 demonstrate a transient increase in intracellular calcium, detected by a Fluo-4 fluorescent signal, in HeLa cells transiently expressing mouse CMKLR1 (mCMKLR1) and $G_{\alpha 15}$ (left) but not in cells transfected with $G_{\alpha 15}$ alone (right). (**C**) Concentration-response curves demonstrate the high potency of NODAGA-CG34 to CMKLR1 which is similar to a natural chemerin-derived peptide ($Chem_{145-157}$) (EC_{50} of 45.7 ± 15.4 nM *vs.* 42.2 ± 3.8 nM, respectively, $P = 0.95$, N = 3 independent experiments). Data are expressed as the mean ± SEM. Statistical significance was calculated using a two-tailed Student's t-test.

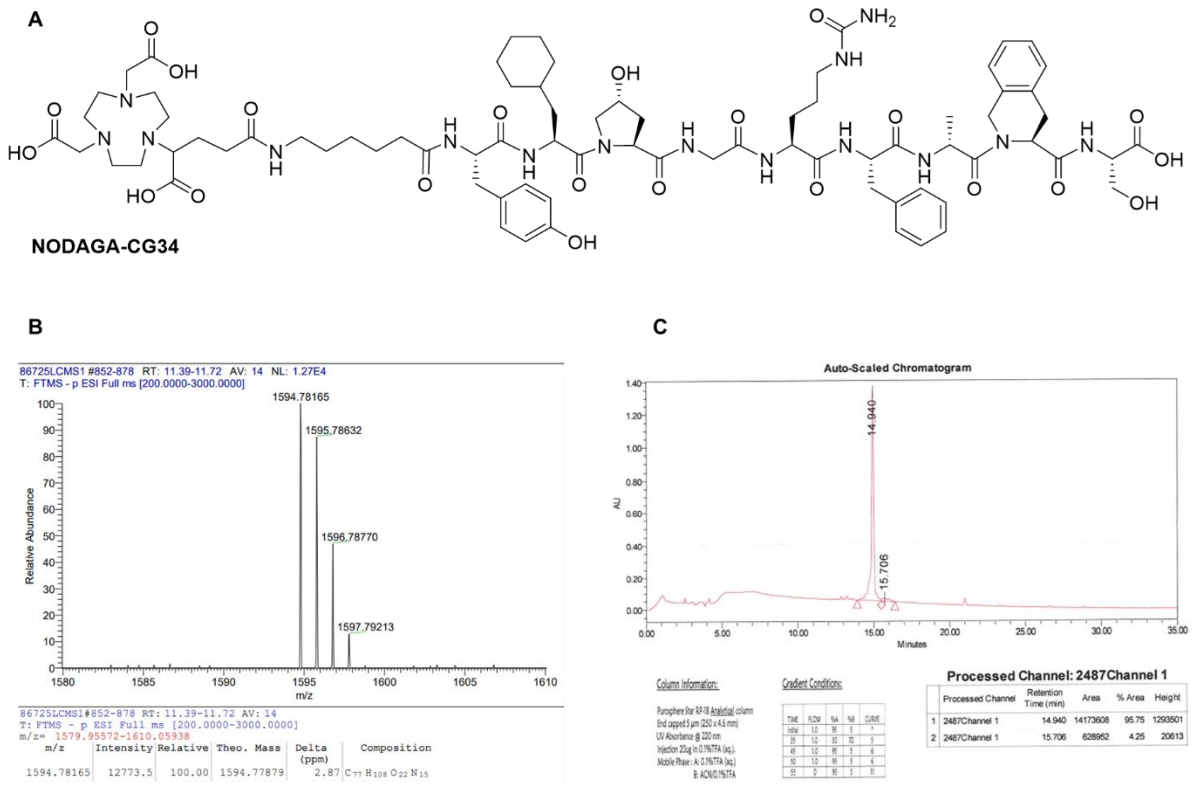

Fig. S2. Confirmation of the identity and purity of NODAGA-CG34. (A) Structure of NODAGA-CG34. **(B)** High resolution mass spectrometry confirms the expected mass and molecular formula of NODAGA-CG34 ($C_{77}H_{108}O_{22}N_{15}$ = 1594.77879, found: 1594.78165). **(C)** The chemical purity (96%) of NODAGA-CG34 is confirmed by analytical reverse-phase high performance liquid chromatography.

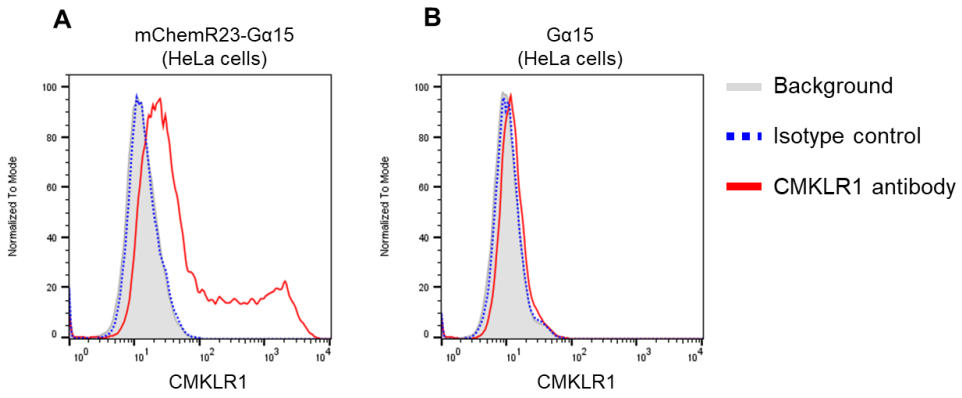

Fig. S3. Surface expression of CMKLR1 in HeLa cells transfected with CMKLR1 and $G_{\alpha 15}$ *vs.* $G_{\alpha 15}$ alone. (A) HeLa cells transiently transfected with mouse CMKLR1 (mCMKLR1) and Gα15 demonstrate surface expression of mCMKLR1 as confirmed by flow cytometry using an anti-mCMKLR1 antibody. **(B)** By contrast, HeLa cells transiently transfected with $G_{\alpha 15}$ alone do not show binding of the anti-mCMKLR1 antibody. N = 3 independent experiments.

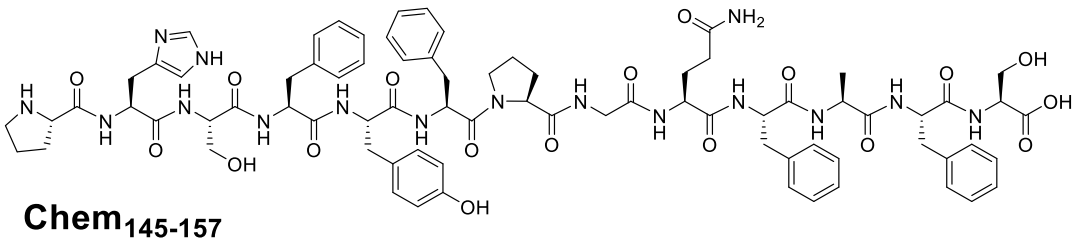

Fig. S4. Structure of Chem145-157 peptide. The structure of $Chem_{145\text{-}157}$ is shown above.

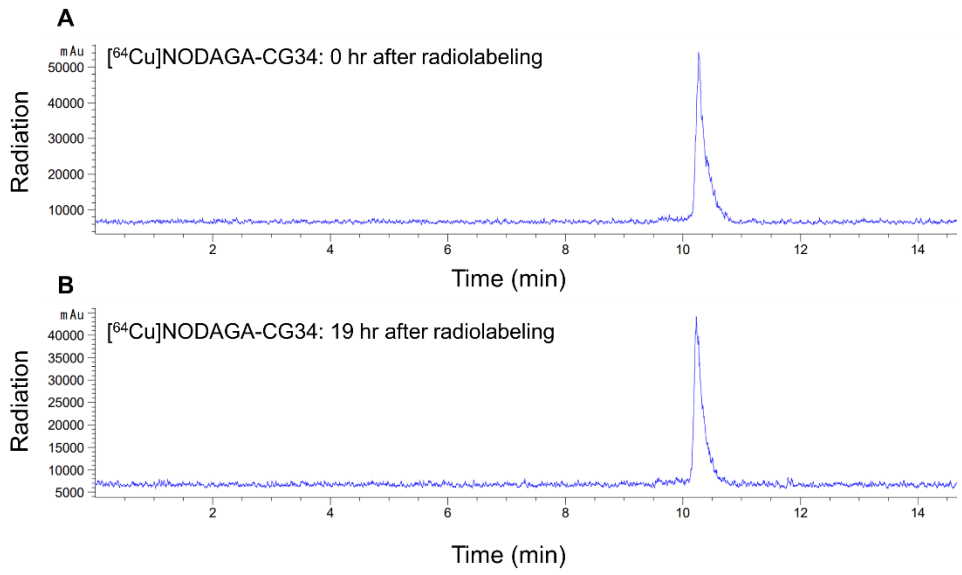

Fig. S5. Stability of [^{64}Cu]NODAGA-CG34. (A) A radio-HPLC immediately following radiolabeling of NODAGA-CG34 with [^{64}Cu]Cu^{+2} shows ~100% radiochemical purity. **(B)** A repeat radio-HPLC after [^{64}Cu]NODAGA-CG34 was stored overnight under ambient conditions shows no new peaks, demonstrating a high degree of stability with no observable radiolysis. N = 2 independent experiments.

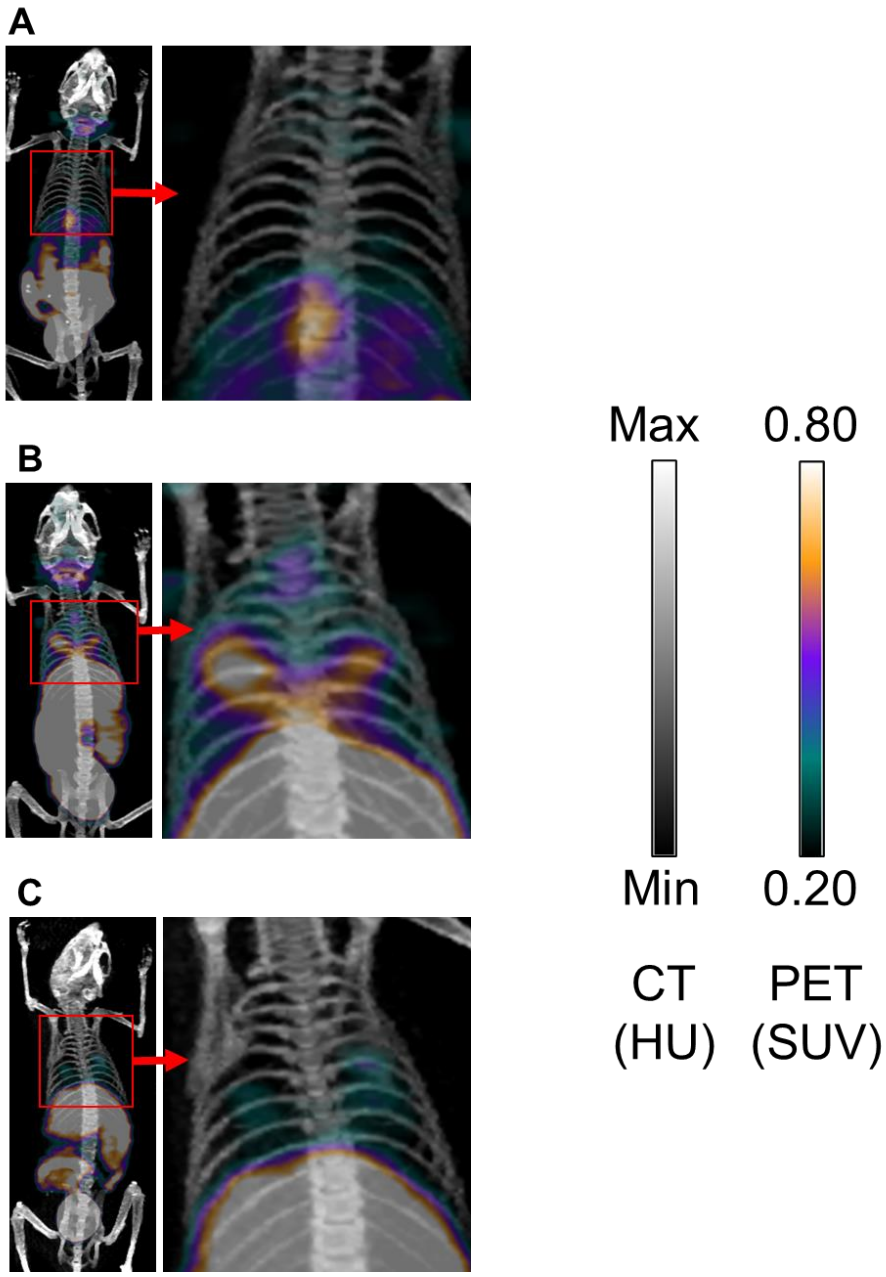

Fig. S6. [^{64}Cu]NODAGA-CG34 PET/CT in LPS-induced lung injury. Maximum intensity projection (MIP) PET/CT images from a control mouse **(A)** *vs.* a mouse at day 2 post-LPS administration **(B)** demonstrate focal areas of increased tracer uptake in ALI. The specificity of tracer uptake is confirmed by co-injection of 100-fold molar excess of non-radiolabeled NODAGA-CG34 which blocks the lung uptake of [^{64}Cu]NODAGA-CG34 in ALI **(C)**. The notable increase in the specific uptake of [^{64}Cu]NODAGA-CG34 in the liver, intestines and spleen of ALI mice is compatible with the induction of a systemic inflammatory response by intra-tracheal LPS.

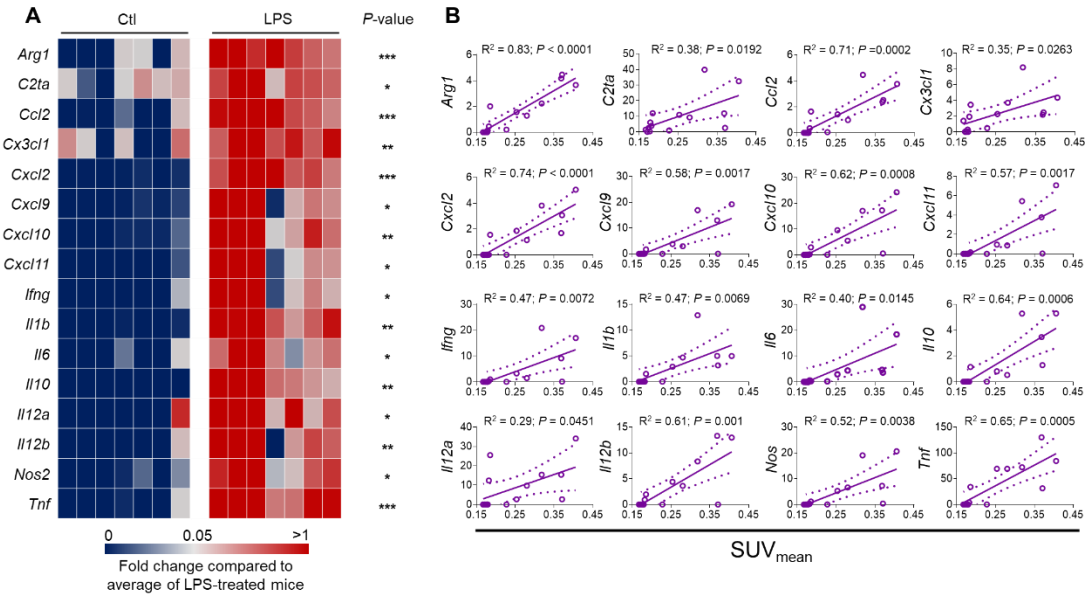

Fig S7. Correlation of [^{64}Cu]NODAGA-CG34 uptake and the expression of inflammatory markers. (**A**) The mRNA expression of multiple inflammatory markers is markedly increased in the lungs two days after induction of LPS-induced experimental lung injury. (**B**) PET-derived quantification of lung [^{64}Cu]NODAGA-CG34 uptake significantly correlates with the expression of multiple inflammatory markers. mRNA transcript levels are normalized to the geometric mean of *Rn18s*, the housekeeping gene. PBS = phosphate buffered saline; LPS = lipopolysaccharide. Linear regressions are shown along with 95% confidence intervals. *P*-values: * < 0.05; ** < 0.01; *** < 0.001; **** < 0.0001. Statistical significance was calculated using a two-tailed Student's t-test. Linear correlations were determined by calculating the Pearson correlation coefficient.

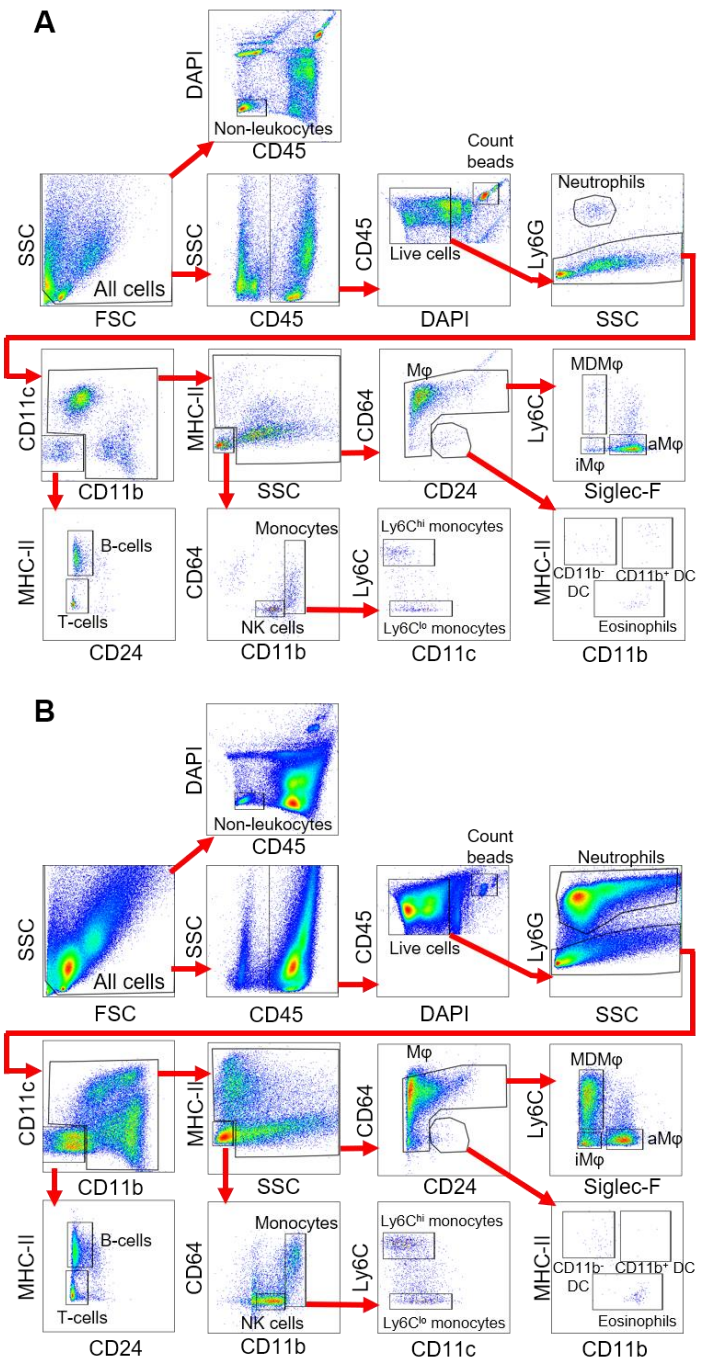

Fig. S8. Flow cytometric gating strategy for identification of major leukocyte subsets in murine lungs. An 11-color flow cytometry panel was adapted for identification of major leukocyte subsets in murine lungs. Representative examples are shown from lungs of PBS **(A)** *vs.* lipopolysaccharide **(B)** treated mice. aMφ: alveolar macrophages; DC: dendritic cells; iMφ: interstitial macrophages; Mφ: macrophages; MDMφ: monocyte-derived macrophages; NK: natural killer cells.

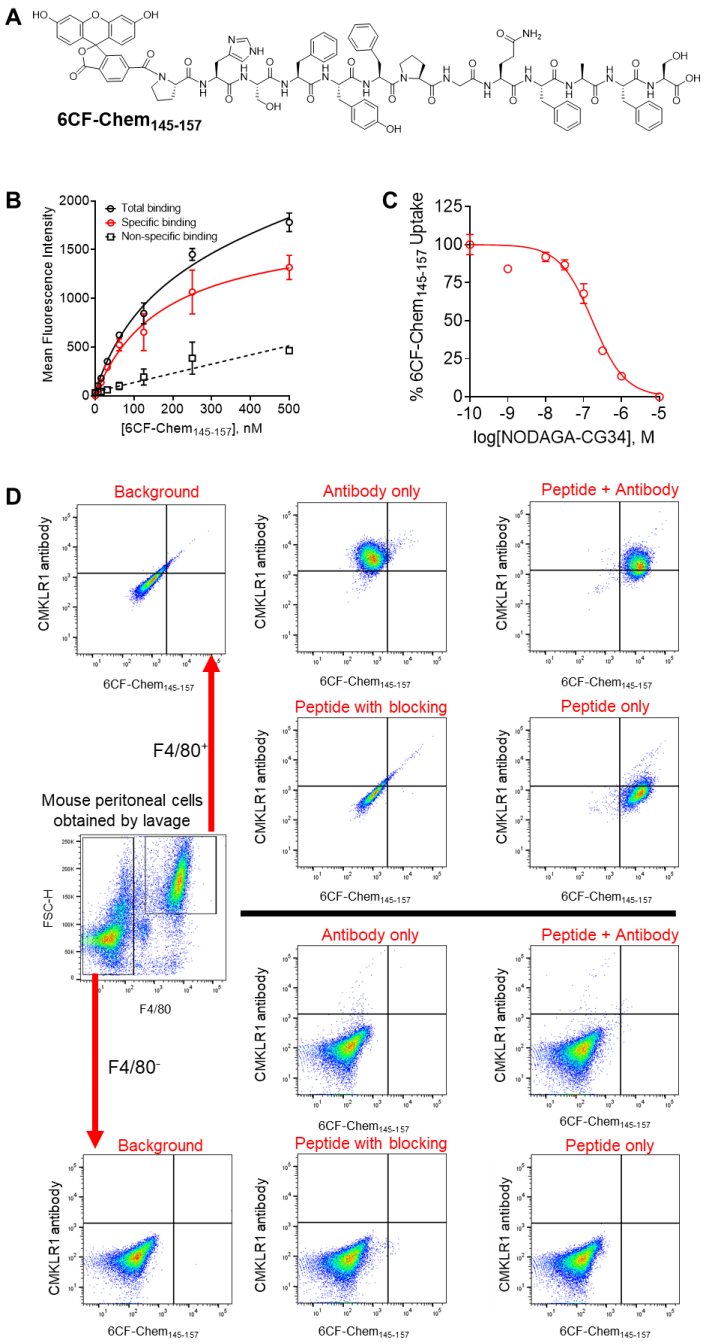

Fig. S9. Specificity of 6CF-Chem$_{145-157}$ for mCMKLR1. (A) The structure of 6CF-Chem$_{145-157}$ is shown. **(B)** The potency (EC_{50}) of 6CF-Chem$_{145-157}$ at mCMKLR1 on F4/80$^+$ peritoneal macrophages is 246.3±48.3 nM (N = 3 independent experiments). **(C)** NODAGA-CG34 competes with 6CF-Chem$_{145-157}$ for binding and uptake at CMKLR1 (IC_{50} = 163.3±21.0 nM; N = 3 independent experiments). **(D)** CMKLR1-expressing F4/80$^+$ peritoneal macrophages demonstrate specific uptake of 6CF-Chem$_{145-157}$. In contrast, there is no binding of 6CF-Chem$_{145-157}$ in the remaining non-macrophage peritoneal cells (F4/80$^-$). Together, these data confirm the specificity and restricted binding of 6CF-Chem$_{145-157}$ to CMKLR1-expressing cells. Blocking studies were conducted by co-incubation of cells with 6CF-Chem$_{145-157}$ and 100-fold excess Chem$_{145-157}$.

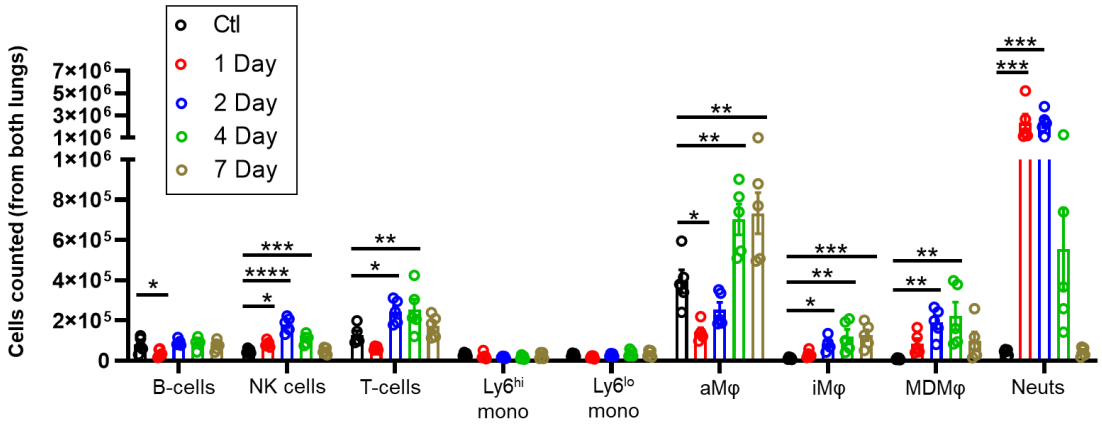

Fig. S10. Kinetics of lung leukocyte populations during LPS-induced ALI as determined by flow cytometry. The absolute cell count for the indicated cell populations at specific time points in lipopolysaccharide (LPS) treated or untreated control mice. Ctl = untreated mice; LPS = lipopolysaccharide; Ly6C^{hi} mono = Ly6C^{hi} monocytes; Ly6C^{lo} mono = Ly6C^{lo} monocytes; aMφ = alveolar macrophages; iMφ = interstitial macrophages; MDMφ = monocyte derived macrophages. n=3 male and n=2 female mice in each group, except for day 2 with n=2 male and n=3 female mice. aMφ: alveolar macrophages; iMφ: interstitial macrophages; MDMφ: monocyte-derived macrophages; NK cells: natural killer cells; Neuts: neutrophils. Data are expressed as the mean ± SEM. *P*-values: * < 0.05; ** < 0.01; *** < 0.001; **** < 0.0001. Statistical significance was calculated using a one-sided ANOVA with a post-hoc two-tailed Fisher's exact test comparing the control group with each treatment group.

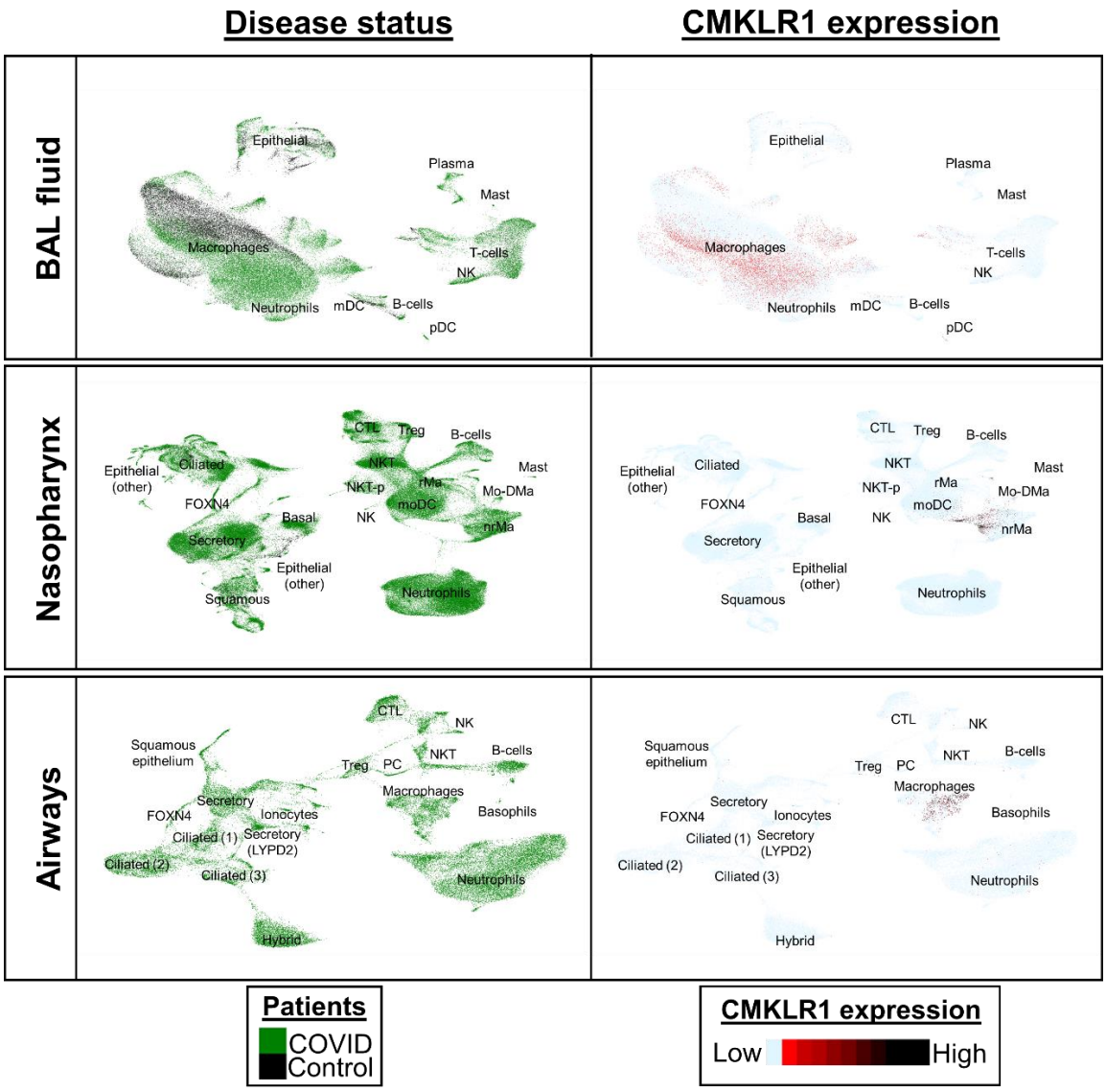

Fig. S11. Increased expression of *CMKLR1* in the respiratory tract of COVID-19 patients is mostly restricted to macrophages. UMAP display of major cell types (left columns) identified from single-cell RNA sequencing of bronchoalveolar (BAL) fluid (top panel), nasopharynx (middle panel) or airway (lower panel) specimens from patients with COVID-19 or SARS-CoV-2-negative healthy controls. The expression of *CMKLR1* in specimens obtained from all three sites is predominantly restricted to macrophages. Moreover, BAL fluid analysis demonstrates a distinct increase in the expression of *CMKLR1* in macrophages of COVID-19 patients compared to those of controls.
The number of patients per panel is as follows: top panel (BAL fluid): N = 9 patients with COVID-19 and 4 healthy controls; middle panel (nasopharynx): N = 19 patients with COVID-19 and 5 healthy controls; and bottom panel (airways): N = 2 patients with COVID-19. The raw and processed data is available in the Gene Omnibus (GSE145926) and European Genome-Phenome Archive (EGAS00001004481) (8, 9). Data was accessed

and analyzed using the UCSC Cell Browser software (11). A link is provided in Table S7 (https://cells-test.gi.ucsc.edu/?ds=ams-supercluster&gene=CMKLR1).

Abbreviations: Ciliated: ciliated epithelial cells; FOXN4: FOXN4^{+} epithelial cells; Secretory: secretory epithelial cells; Squamous: squamous epithelial cells; rMa: resident macrophages; moDC: monocyte-derived dendritic cells; nrMa: non-resident macrophages; Treg: regulatory T-cells; CTL: cytotoxic T-cells; NKT: natural killer T-cells; NKT-p: proliferating natural killer T-cells; NK: natural killer cells; Neu: neutrophils; pDC: plasmacytoid dendritic cells; MC: mast cell; mDC: myeloid dendritic cells.

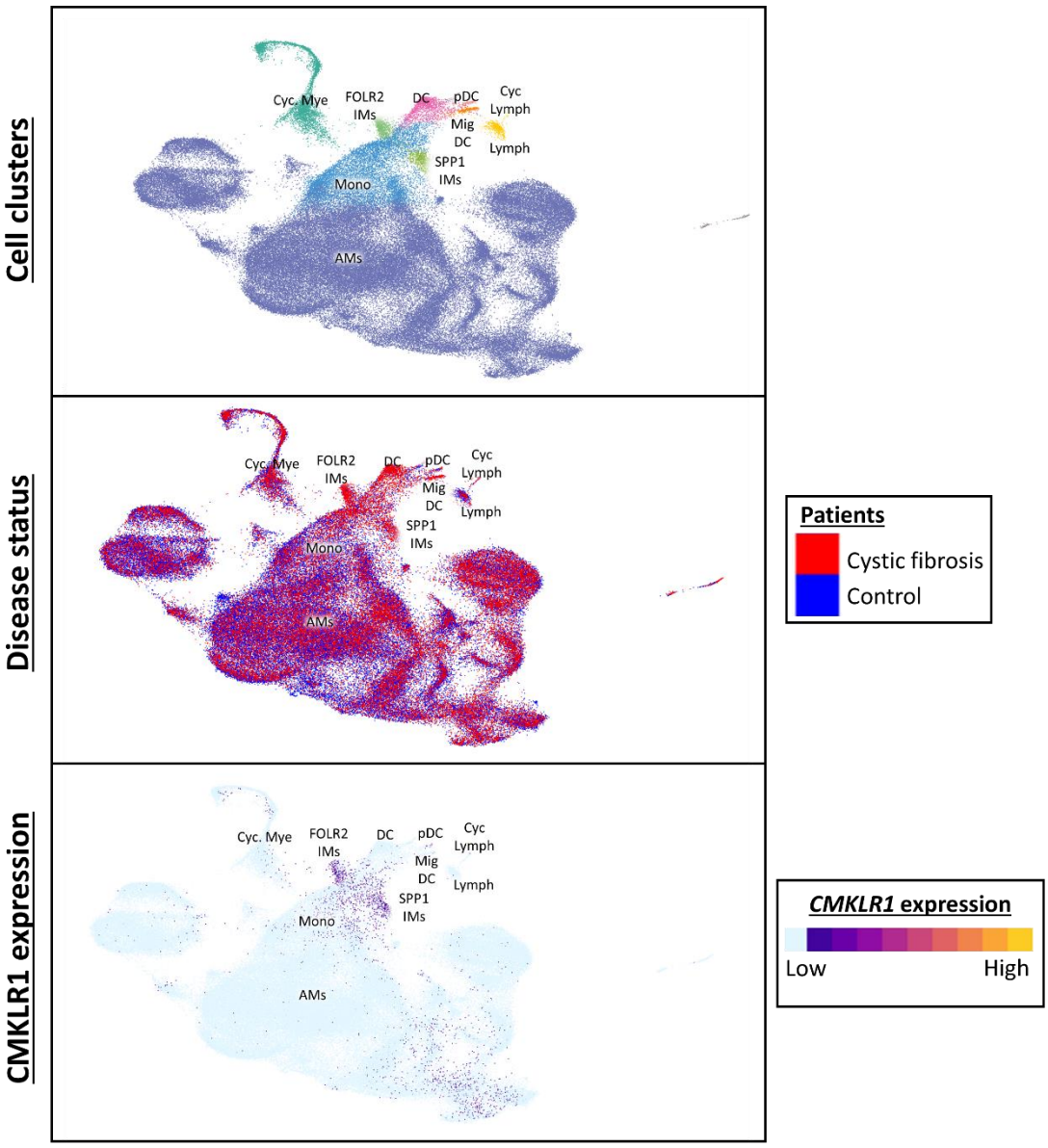

Fig. S12. Restricted expression of *CMKLR1* by macrophages in bronchoalveolar fluid specimens from patients with cystic fibrosis. UMAP display of major cell types identified from single-cell RNA sequencing of bronchoalveolar lavage (top panel) and their distribution by disease status (middle panel) in three patients with mild cystic fibrosis and four healthy control participants. *CMKLR1* expression (bottom panel) was predominantly restricted to FOLR2^{+} and SPP1^{+} interstitial macrophages in patients with cystic fibrosis with less abundant expression in monocytes and macrophages. The raw and processed data is available in the Gene Omnibus (GSE193782) (10). Data was accessed and analyzed using the UCSC Cell Browser website (11). A link is provided in Table S7 (https://cells-test.gi.ucsc.edu/?ds=ams-supercluster&gene=CMKLR1).

Abbreviations: AMs: alveolar macrophages; Cyc Lymph: lymphoid cycling cells; FOLR2 IM: FOLR2^{+} interstitial macrophages; SPP1 IM: SPP1^{+} interstitial macrophages; Mig DC: migratory dendritic cells; pDC: plasmacytoid dendritic cells; Lym: lymphocytes.

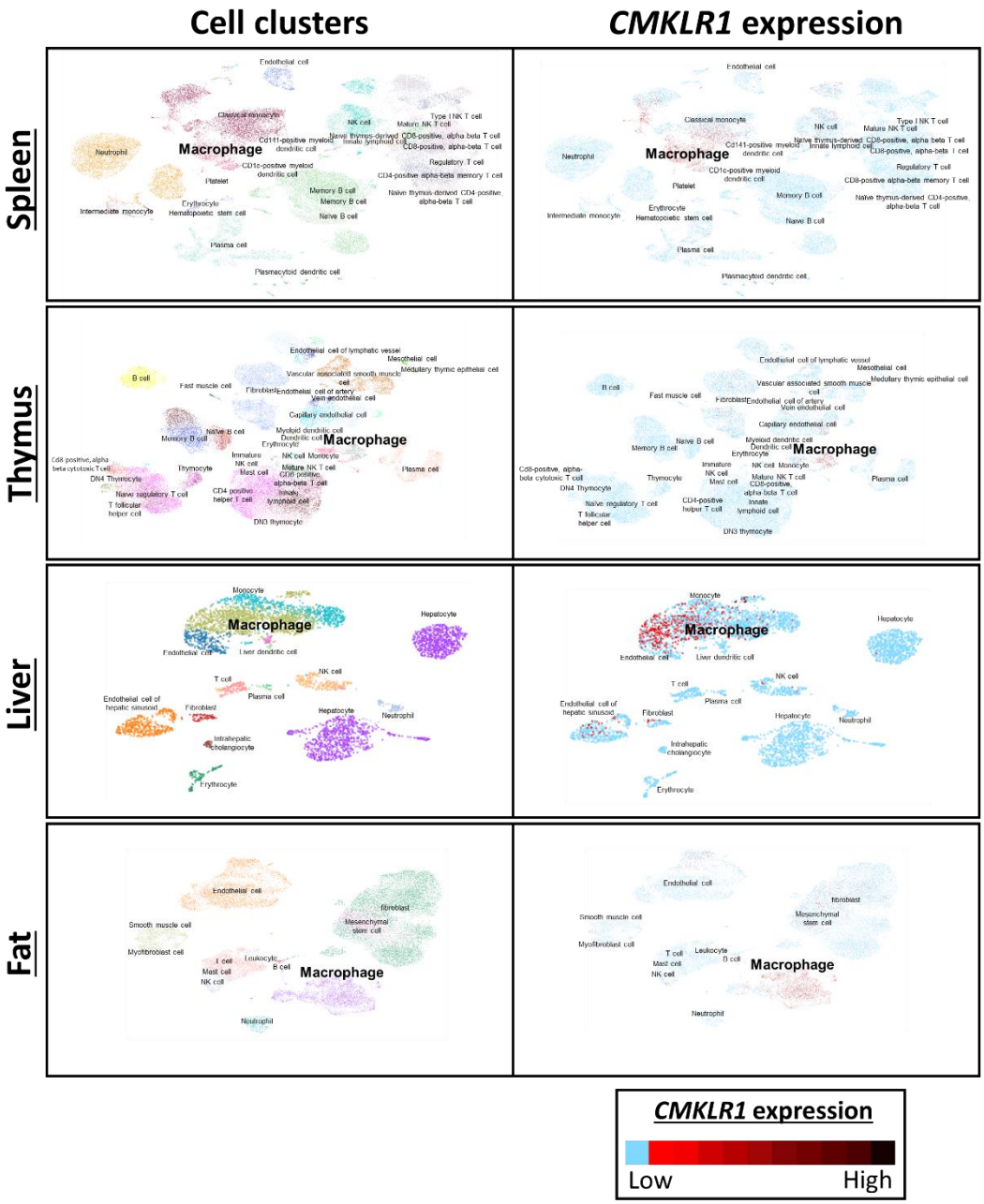

Figure S13. *CMKLR1* is predominantly expressed on macrophages in various non-pulmonary tissues. UMAP display of major cell types identified from single-cell RNA sequencing of the indicated tissue (left panel) and their *CMKLR1* expression (right panel) in donor tissue. *CMKLR1* expression was largely restricted to macrophages. The raw and processed data is available in the Gene Omnibus (GSE201333). Data was accessed and analyzed using the UCSC Cell Browser website (11). Links to the data are provided in Table S7.

Abbreviations: AMs: alveolar macrophages; Cyc Lymph: lymphoid cycling cells; FOLR2 IM: FOLR2^{+} interstitial macrophages; SPP1 IM: SPP1^{+} interstitial macrophages; Mig DC: migratory dendritic cells; pDC: plasmacytoid dendritic cells; Lym: lymphocytes.

Table S1. List of general reagents.

Reagent	Company	Catalog #
Black 96-well plate	Thermo Fisher	165305
C57BL/6 plasma	Innovative Research	IGMSC57PLAK2E10ML
Cell strainer (70 um)	VWR	10199-656
Clear 96-well plate	Fisher	FB012931
Dexamethasone	Fresenius Kabi USA	500601
DMEM	Thermo Fisher	10566016
DNase I	Sigma	D4527-10KU
Fetal bovine serum	Gibco	10082147
Fluo-4 AM	Thermo Fisher	F14201
G50 Microspin column	GE	27-5330-01
HBSS with Ca^{+2} and Mg^{+2}	Gibco	14025-076
Lipofectamine 3000	Thermo Fisher	L3000008
Lipopolysaccharide	Millipore Sigma	437627
Low retention tubes (radiolabeling)	Eppendorf	022431081
Qiagen Plasmid Maxi Kit	Qiagen	12162
PBS	Lonza	17-512F
Penicillin/streptomycin	Gibco	15070-063
Pluronic F-127	Millipore Sigma	P2443
Poly-D-lysine	Thermo Fisher	A3890401
Protease Inhibitor	Thermo Fisher	A32963
RBC Lysis Buffer (10X)	Biolegend	420301
QuantiTect Reverse Transcription Kit	Qiagen	205313
Rodent Intubation Stand	Braintree Scientific	RIS 100
Taqman Master Mix	Thermo Fisher	4369510
Trizol	Thermo Fisher	15596026

Table S2. Plasmids for transient transfections.

Plasmid	Company	Catalog
$G_{\alpha 15}$	cDNA Resource Center	GNA1500000
mCMKLR1	Origene	MC208581

Table S3. Radio-HPLC methods (Agilent 1260 Infinity HPLC, C18 Luna Analytical Column).

Time (min)	**Solvent 1 (%)** (H_2O with 0.1% v/v trifluoroacetic acid)	**Solvent 2 (%)** (Acetonitrile with 0.1% v/v trifluoroacetic acid)	**Flow rate (mL/min)**
0	100	0	2.0
5	95	5	2.0
15	5	95	2.0

Table S4. List of reagents used for flow cytometry.

Reagent	Assay	Company	Catalog #
Anti-CCR2-Fluorescein	Flow cytometry	R&D Biosystems	FAB5538F-100
Anti-CD11b-PE	Flow cytometry	BioLegend	101208
Anti-CD11c-PerCP	Flow cytometry	BioLegend	117326
Anti-CD24-AF700	Flow cytometry	BioLegend	101836
Anti-CD45-BV421	Flow cytometry	BioLegend	103134
Anti-CD64-APC	Flow cytometry	BioLegend	139306
Anti-CMKLR1-AF488	Flow cytometry	R&D Biosystems	FAB7610G
Anti-Ly6C-APC-Cy7	Flow cytometry	BioLegend	128026
Anti-Ly6G-BV395	Flow cytometry	BD Biosciences	563978
Anti-MHC-II-BV605	Flow cytometry	BioLegend	107639
Anti-SiglecF-BV510	Flow cytometry	BD Biosciences	740158
DAPI	Flow cytometry	BD Biosciences	564907
IgG_{2B} isotype control-AF488	Flow cytometry	R&D Biosystems	IC013G
IgG_{2B} isotype control-fluorescein	Flow cytometry	R&D Biosystems	IC013F
Mouse Fc block	Flow cytometry	BD Pharmingen	553141
Precision count beads	Flow cytometry	BioLegend	424902

Table S5. List of reagents used for immunofluorescent histology.

Antibody	Assay	Company	Catalog #
Anti-rabbit IgG (H+L) - Cy5	Immunofluorescence	Jackson ImmunoResearch	711-175-152
Anti-rat IgG (H+L) - Cy3	Immunofluorescence	Jackson ImmunoResearch	712-165-150
ProLong Gold Antifade Mountant with DAPI	Immunofluorescence	Thermo Fisher	P36931
Rabbit anti-mouse CMKLR1	Immunofluorescence	LSBio	B12924
Rat anti-mouse CD45	Immunofluorescence	BioLegend	103101
Rat anti-mouse F4/80	Immunofluorescence	Thermo Fisher	14-4801-81
Rat anti-mouse Ly6G	Immunofluorescence	BioLegend	127601

Table S6. List of mouse primers used for quantitative RT-PCR.

Assay Name	Gene	Assay ID
Arg1	Arginase 1	Mm00475988_m1
Ccl2	C-C motif chemokine ligand 2	Mm00441242_m1
Ciita	Class II major histocompatibility complex transactivator	Mm00482914_m1
Cx3cl1	C-X3-C motif chemokine ligand 1	Mm00436454_m1
Cxcl10	C-X-C motif chemokine ligand 10	Mm00445235_m1
Cxcl11	C-X-C motif chemokine ligand 11	Mm00444662_m1
Cxcl2	C-X-C motif chemokine ligand 2	Mm00436450_m1
Cxcl9	C-X-C motif chemokine ligand 9	Mm00434946_m1
Ifng	Interferon-γ	Mm01168134_m1
Il10	Interleukin 10	Mm01288386_m1
Il12a	Interleukin 12A	Mm00434169_m1
Il12b	Interleukin 12B	Mm00434174_m1
Il1b	Interleukin 1β	Mm00434228_m1
Il6	Interleukin 6	Mm00446190_m1
Nos2	Nitric oxide synthase 2	Mm00440502_m1
Rn18s	18S ribosomal RNA	Mm03928990_m1
Tnf	Tumor necrosis factor	Mm00443258_m1

Table S7. Single-cell RNA-seq datasets for CMKLR1 expression.

Sample	Disease	Direct link for dataset	Figure	Ref
Bronchoalveolar lavage	COVID-19	https://cells-test.gi.ucsc.edu/?ds=covid19-balf&gene=CMKLR1	Fig. S11	(8)
Nasopharynx	COVID-19	https://cells-test.gi.ucsc.edu/?ds=covid-airways+nasopharynx&gene=CMKLR1	Fig. S11	(9)
Airways	COVID-19	https://cells-test.gi.ucsc.edu/?ds=covid-airways+all&gene=CMKLR1	Fig. S11	(9)
Bronchoalveolar lavage	Cystic fibrosis	https://cells-test.gi.ucsc.edu/?ds=ams-supercluster&gene=CMKLR1	Fig. S12	(10)
Spleen	Various	https://cells.ucsc.edu/?ds=tabula-sapiens+by-organ+spleen	Fig. S13	(12)
Thymus	Various	https://cells.ucsc.edu/?ds=tabula-sapiens+by-organ+thymus&gene=CMKLR1	Fig. S13	(12)
Liver	Various	https://cells.ucsc.edu/?ds=tabula-sapiens+by-organ+liver&gene=CMKLR1	Fig. S13	(12)
Fat	Various	https://cells.ucsc.edu/?ds=tabula-sapiens+by-organ+fat&gene=CMKLR1	Fig. S13	(12)

References

1. S. Tavakoli *et al.*, Differential Regulation of Macrophage Glucose Metabolism by Macrophage Colony-stimulating Factor and Granulocyte-Macrophage Colony-stimulating Factor: Implications for (18)F FDG PET Imaging of Vessel Wall Inflammation. *Radiology* **283**, 87-97 (2017).
2. G. Barnea *et al.*, The genetic design of signaling cascades to record receptor activation. *Proc Natl Acad Sci U S A* **105**, 64-69 (2008).
3. J. Haddad *et al.*, Molecular Imaging of Very Late Antigen-4 in Acute Lung Injury. *J Nucl Med* **62**, 280-286 (2021).
4. W. Beaino, C. J. Anderson, PET imaging of very late antigen-4 in melanoma: comparison of 68Ga- and 64Cu-labeled NODAGA and CB-TE1A1P-LLP2A conjugates. *J Nucl Med* **55**, 1856-1863 (2014).
5. J. Toms *et al.*, Targeting Fibroblast Activation Protein: Radiosynthesis and Preclinical Evaluation of an (18)F-Labeled FAP Inhibitor. *J Nucl Med* **61**, 1806-1813 (2020).
6. J. C. Melms *et al.*, A molecular single-cell lung atlas of lethal COVID-19. *Nature* **595**, 114-119 (2021).
7. Y. Hao *et al.*, Integrated analysis of multimodal single-cell data. *Cell* **184**, 3573-3587 e3529 (2021).
8. M. Liao *et al.*, Single-cell landscape of bronchoalveolar immune cells in patients with COVID-19. *Nat Med* **26**, 842-844 (2020).
9. R. L. Chua *et al.*, COVID-19 severity correlates with airway epithelium-immune cell interactions identified by single-cell analysis. *Nat Biotechnol* **38**, 970-979 (2020).
10. X. Li *et al.*, ScRNA-seq expression of IFI27 and APOC2 identifies four alveolar macrophage superclusters in healthy BALF. *Life Sci Alliance* **5** (2022).
11. M. L. Speir *et al.*, UCSC Cell Browser: Visualize Your Single-Cell Data. *Bioinformatics* 10.1093/bioinformatics/btab503 (2021).
12. C. Tabula Sapiens *et al.*, The Tabula Sapiens: A multiple-organ, single-cell transcriptomic atlas of humans. *Science* **376**, eabl4896 (2022).